Droplet Size Distributions of Liquid-Liquid Dispersions in Centrifugal Pumps

Philipp Schmitt[1,†], Stephan Sibirtsev[2,†], Mark W. Hlawitschka[1], Robert Styn[2], Andreas Jupke[2], and Hans-Jörg Bart[1,*]

DOI: 10.1002/cite.202000180

This is an open access article under the terms of the Creative Commons Attribution License, which permits use, distribution and reproduction in any medium, provided the original work is properly cited.

Supporting Information
available online

Dedicated to Prof. Dr.-Ing. Matthias Kraume on the occasion of his 65th birthday

The generation of liquid-liquid dispersions with defined droplet size distributions is an important aspect for process equipment design. In this work, two centrifugal pumps with different impeller diameters were used to generate dispersions at selected operating points for a paraffin oil-water system. The droplet break-up phenomena within the centrifugal pumps were analyzed using a transparent pump design in combination with high-speed imaging. Droplet size distributions at centrifugal pump discharge nozzle were recorded with optical probe measurement technologies and evaluated by means of image processing using a neural network. The influence of impeller diameter, rotational speed, volumetric flow rate and dispersed phase fraction are discussed. Experimental data is correlated using fluid properties, operating data as well as centrifugal pump dimensions. The correlations developed from results of this work serve as a basis for the equipment design of centrifugal pumps.

Keywords: Centrifugal pump, Droplet size distribution, Liquid-liquid dispersion, Turbulent particle break-up, Weber number

Received: August 11, 2020; *revised:* October 30, 2020; *accepted:* November 18, 2020

1 Introduction

Dispersing, conveying and separation of liquid-liquid (L/L) multiphase flow are essential operations in chemical industry. For the generation of dispersions from two coherent liquids, mainly agitators, perforated dividers or static mixers are used. Various pump types are used for the conveyance of fluid phase systems. Centrifugal pumps are preferred in industry because of their simple design, low price and robustness [1]. For the coalescing of fluid phase systems, gravitational or centrifugal separators are used depending on the separation input. Furthermore, centrifugal extractors are used combining the mixing and separating apparatus in one device. Studies focus on the experimental investigation and model-based description of the droplet break-up and coalescence phenomena in the centrifugal field [2, 3]. Instead of a pure pumping action the centrifugal pump can be used for two-phase mixing, thus combines two modes of action, pumping and mixing, as a one-device solution [4]. This results in a high potential for process intensification and for improving the economic efficiency of L/L processes.

For centrifugal pumps, extensive literature exists concerning the investigation of single-phase flows and the determination of the pump performance [5, 6]. In pump design and selection of the operating range, attention is paid to the issue of cavitation, which has a vast influence on efficiency and may cause significant pump damage [7, 8]. With the increased use of high-performance computers, simulation-based methods such as computational fluid dynamics (CFD) for optimizing, e.g., pressure loss and pump performance have come into focus in recent decades. Comprehensive overviews are given in [9, 10].

---

[1] Philipp Schmitt, Dr.-Ing. Mark W. Hlawitschka,
Prof. Dipl.-Ing. Dr. techn. Hans-Jörg Bart
bart@mv.uni-kl.de
Technische Universität Kaiserslautern, Chair of Separation Science and Technology, Gottlieb-Daimler-Straße 44, 67663 Kaiserslautern, Germany.

[2] Stephan Sibirtsev, Robert Styn, Prof. Dr.-Ing. Andreas Jupke
RWTH Aachen University, Fluid Process Engineering (AVT.FVT), Forckenbeckstraße 51, 52074 Aachen, Germany.

† These author contributed equally.

While single-phase flows have already been extensively analyzed, only preliminary investigations are known in the field of two-phase systems. Several researchers were able to demonstrate the change of the pump head and the hydraulic loss due to air admission using hydraulic performance tests [11, 12]. Furthermore, Murakami and Minemura investigated the influence of energy input, phase ratio of a gas-liquid system as well as impeller design parameters on the size distribution of gas bubbles produced in centrifugal pumps experimentally [11].

For the L/L systems, centrifugal pumps are able to produce both, dispersion and separation, depending on material system, design and operational parameters. This effect is already industrially applied. For instance, several important process steps in the cleavage of cumene hydroperoxide in 40 wt % sulfuric acid to phenol and acetone use centrifugal pumps as a mixing device [4]. Experiments on the quantification of L/L dispersions in centrifugal pumps and experiments on oil drop motion in impellers have revealed the effects of droplet break-up in centrifugal pumps [13, 14]. In petroleum production and transportation, centrifugal pumps cause dispersed water droplets to be broken into smaller droplets by shear effects. Dabirian et al. [15] summarizes available models from literature for the calculation of droplet sizes and distributions.

To our knowledge, a systematic scientific study to predict the dispersion production and separation in centrifugal pumps has not yet been carried out. Dispersion production as well as separation by means of centrifugal pumps can neither be used nor avoided in a targeted manner at the present state of the art.

The dispersing or coalescing effect in centrifugal pumps can be used industrially in a targeted application, if there is an understanding of L/L fluid dynamics regarding the operating conditions, pump geometry and material system parameters. This can reduce equipment effort for L/L extraction plants and intensify extraction processes. The production of a dispersion is dependent on the mechanical impeller action. Droplet break-up and coalescence take place continuously inside the apparatus. At constant operating conditions a stationary dynamic equilibrium is established, which depends on the physical properties of the involved liquids. Depending on the operating conditions, this dynamic equilibrium is characterized by a reproducible droplet size distribution (DSD).

The basics of droplet break-up are related to investigations in stirred tanks [16–18]. Droplet break-up is caused by external destabilizing forces acting on the droplet. These forces arise from the turbulent kinetic energy of the continuous phase. They may have their origin in viscous stresses or dynamic pressures acting in the enclosing continuous phase. Droplet stabilizing forces are described by the interfacial force and the viscous force of the dispersed phase. The ratio between the external force and the interfacial force of the droplet is described by the Weber number [19]. The significant work of many researchers has led to the development of semi-empirical correlations of mean diameters using the Weber number and geometry-dependent fit parameters. [16, 17, 19]

In the present work, L/L fluid dynamics in centrifugal pumps is explained and described using correlations from literature. It is shown that with adapted Weber number correlations it is possible to estimate resulting DSDs of L/L dispersions at the pump outlet.

2 Fundamentals

In this section, all theoretical fundamentals necessary for the understanding of the model-based description of droplet break-up phenomena in centrifugal pumps are explained.

2.1 Energy Dissipation Rate

The model-based description of droplet break-up phenomena during the mixing process in a centrifugal pump can be conducted analogously to the description of these phenomena during the mixing process in a stirred tank because of analogous impeller design. For mixing apparatuses, the average energy dissipation rate $\bar{\varepsilon}$ is proportional to the dissipation power P_{diss} per unit mass required to agitate the material system [15, 16]:

$$\bar{\varepsilon} = \frac{P_{\mathrm{diss}}}{V \rho_{\mathrm{c}}} \tag{1}$$

In centrifugal pumps, the dissipation power P_{diss} is described as the difference between the power input P'_{shaft} and the pump power output $P_{\dot{\mathrm{Q}}}$, where V is assumed to be the entire pump volume from the inlet to the outlet of the pump:

$$\bar{\varepsilon} = \frac{P'_{\mathrm{shaft}} - P_{\dot{\mathrm{Q}}}}{V \rho_{\mathrm{c}}} = \frac{M'_{\mathrm{shaft}} 2\pi n - \Delta p \dot{Q}}{V \rho_{\mathrm{c}}} \tag{2}$$

In Eq. (2), M'_{shaft} is the torque at the pump shaft less bearing and pump sealing friction torque, n is the rotational speed of the pump impeller, $\dot{Q}$ is the volumetric flow rate, Δp the pressure drop between the inlet and the outlet of the pump and ρ_{c} the continuous phase density. With the knowledge of the material system, design and operating parameters as well as the experimental determination of the torque and the pressure drop, Eq. (2) can be used to determinate the averaged energy dissipation rate from experimental data.

If the torque at the pump shaft cannot be determined experimentally, further models can be utilized to calculate the averaged energy dissipation rate $\bar{\varepsilon}$. Pereyra [20] applied two different models to calculate $\bar{\varepsilon}$ for centrifugal pumps. The first method is based on the functional relationship between averaged energy dissipation rate and dissipated energy within the centrifugal pump, which can be calculated from the pressure drop Δp, the volumetric flow rate of the L/L dispersion $\dot{Q}$, the dispersion density ρ_m, and the pump volume V:

$$\bar{\varepsilon} = C_1 \frac{\Delta p \dot{Q}}{V \rho_\mathrm{m}} \tag{3}$$

The alternative method describes the droplet break-up by modeling the averaged energy dissipation rate $\bar{\varepsilon}$ at the blade trailing edge as a function of rotational speed n and the impeller outlet diameter D_2:

$$\bar{\varepsilon} = C_2 n^3 D_2^2 \tag{4}$$

However, studies have shown that droplet break-up in centrifugal pumps occurs mainly at the blade leading edge [11, 14]. When a fluid enters the pump impeller without pre-rotation, the relative speed between impeller and fluid at the leading edge is equal to the circumferential speed. The initial break-up of the droplets entering the impeller eye is high enough that almost no further break-up occurs at the impeller trailing edge. Therefore, the averaged energy dissipation rate $\bar{\varepsilon}$ can also be described proportional to the blade inlet diameter D_1.

$$\bar{\varepsilon} = C_3 n^3 D_1^2 \tag{5}$$

In any case a fitting parameter C_i needs to be adapted to experimental data. For this reason, the functional relationship between averaged energy dissipation rate and the maximum stable droplet diameter d_max has to be considered.

2.2 Maximum Stable Droplet Diameter

In a two-phase flow, the L/L dispersion can be characterized by the maximum stable droplet diameter d_max. The maximum stable droplet diameter d_max is defined to be equal to the droplet size belonging to 95 % of the cumulative volume and can be obtained from the corresponding cumulative distribution curve [21].

Several authors propose models based on experimental studies to predict d_max under shear effects in a turbulent flow. For isotropic turbulence, Kolmogorov considered the turbulent eddy sizes and suggested that the maximum stable droplet diameter d_max is equal to the size of the eddy. Hence, according to Kolmogorov's theory the maximum stable droplet diameter d_max is dependent on the average energy dissipation rate $\bar{\varepsilon}$ and can be received from Eq. (6), where $\bar{u}_\mathrm{c}$ is the average fluctuation velocity:

$$\bar{u}_\mathrm{c}^2 = C_4 (\bar{\varepsilon} d_\mathrm{max})^{2/3} \tag{6}$$

Hinze [19] proposed that the break-up of a fluid particle depends on the ratio of the inertial stress of the continuous liquid to the interfacial stress of the dispersed phase. If this ratio exceeds a critical value, the possibility of droplet break-up increases. Based on Kolmogorov's equation for the fluctuation velocity, Hinze suggested the critical Weber number to define and calculate this critical value (Eq. (7)).

$$We_\mathrm{crit} = \frac{\tau_\mathrm{inertial}}{\tau_\mathrm{interfacial}} = \frac{\rho_\mathrm{c} \bar{u}_\mathrm{c}^2}{\sigma / d_\mathrm{max}} = \frac{\rho_\mathrm{c} C_4 \bar{\varepsilon}^{2/3} d_\mathrm{max}{}^{5/3}}{\sigma} \tag{7}$$

Moreover, Hinze used experimental data to determine the critical Weber number to 1.18. With Weber numbers greater than We_crit, droplet break-up occurs. For the maximum stable droplet diameter d_max and $C_4 \approx 2.0$ he suggested the following expression:

$$d_\mathrm{max} = \left(\frac{We_\mathrm{crit}}{2}\right)^{3/5} \left(\frac{\sigma}{\rho_c}\right)^{3/5} \bar{\varepsilon}^{(-2/5)} \tag{8}$$

As the model of Hinze does not consider the effect of the viscous force, it is only valid if the viscosity of the dispersed phase is smaller or equal to the viscosity of the continuous phase. To extend the validity range of the model to higher disperse-phase viscosities μ_D, Davies [22] modified Hinze's model by adding a term for the viscous force in the dispersed phase, which results in Eq. (9). In Davies' expression for the maximum stable droplet diameter d_max, We_crit is equal to 1:

$$d_\mathrm{max} = We_\mathrm{crit}^{3/5} \left(\frac{\sigma}{\rho_\mathrm{c}} + \frac{\mu_\mathrm{D} (\bar{\varepsilon} d_\mathrm{max})^{1/3}}{4 \rho_\mathrm{c}}\right)^{3/5} \bar{\varepsilon}^{(-2/5)} \tag{9}$$

A further development of the model was performed by Pereyra [20] who specified the critical Weber number as the ratio of disruptive shear stress in the continuous phase to cohesive shear stress in the dispersed phase and suggested the definition of the maximum stable droplet diameter d_max as following:

$$d_\mathrm{max} = We_\mathrm{crit} \left(\frac{\left(\sigma + 2^{-3/2} \mu_\mathrm{D} (\bar{\varepsilon} d_\mathrm{max})^{1/3}\right)^{3/5}}{\rho_\mathrm{d}^{1/5} \rho_\mathrm{c}^{2/5}}\right) \bar{\varepsilon}^{(-2/5)} \tag{10}$$

Based on 169 experimental data points of experimental investigations on droplet break-up in static mixers, jets and pipes, for his model Pereyra defined the critical Weber number to $We_\mathrm{crit} = 0.9$

Dabirian et al. [15] used both models for calculation of the averaged energy dissipation rate (Eq. (3) and (4)) in combination with the models for the maximum stable droplet diameter (Eqs. (8)–(10)) to predict the maximum stable droplet diameter and to compare the simulation and experimental results. Dabirian et al. have proved that the model suggested by Pereyra [20] in combination with the rotational speed dependent model for the averaged energy dissipation rate (Eq. (4)) predicts the most accurate results for the maximum stable droplet diameter in combination with the description of the averaged energy dissipation rate from Eq. (4).

2.3 Sauter Mean Diameter

The Sauter mean diameter (SMD) d_{32} is of particular interest as it represents the mean diameter of the entire DSD. With the knowledge of the nominal diameter d_i and the number n_i of droplets in a size class i, the SMD can be calculated using Eq. (11) [23], where M is the number of size classes describing the DSD.

$$d_{32} = \frac{\sum_{i=1}^{M} d_\mathrm{i}^3 n_\mathrm{i}}{\sum_{i=1}^{M} d_\mathrm{i}^2 n_\mathrm{i}} \tag{11}$$

In a stirred tank, droplets of a L/L dispersion in a two-phase flow are stabilized by the surface energy $4\pi d^2\sigma$ and destabilized with respect to their droplet size d by the turbulent energy $\frac{4}{3}\pi d^3\rho_\mathrm{c}\varepsilon$ of the surrounding flow field. Where σ is the interfacial tension and ε the local energy dissipation rate. The probability $P(d)$ that a droplet of size d exists in balance between cohesive and disruptive forces can be described by the ratio of the turbulent energy and the surface energy [16]:

$$P(d) = \varphi\left(\frac{\frac{4}{3}\pi d^3\rho_\mathrm{c}\int_{1/D}^{\infty} E(k)\mathrm{d}k}{4\pi d^2\sigma}\right) \tag{12}$$

Here, φ represents an unknown functional relationship between both energies. $E(k)$ is the energy spectrum function and k is the wave number. Only the part of the energy scale that contains wave numbers larger than $1/d$ is considered. If the flow is not strongly affected by viscous forces, the energy spectrum function $E(k)$ can essentially be described as follows [24]:

$$E(k) = C_5\varepsilon^{2/3}k^{-5/3} \tag{13}$$

where C_5 is a constant. The integration of Eq. (13) in Eq. (12) leads to a description of the probability $P(d)$:

$$P(d) = \varphi\left(\frac{C_5}{2}\frac{\rho_\mathrm{c}}{\sigma}\varepsilon^{2/3}d^{5/3}\right) \tag{14}$$

It is assumed, that a significant part of the total energy dissipation takes place at the blade leading edge of the centrifugal pump at sufficiently large Reynolds numbers (Eq. (5)), With Eq. (14), this leads to a correlation that describes a droplet with the probability $P(d)$ with certain size directly dependent on the Weber number.

$$P(d) = \varphi\left(\frac{\rho_\mathrm{c}N^2D_1^{4/3}d^{5/3}}{\sigma}\right) = \varphi\left(\frac{d}{D_1}We^{3/5}\right) \tag{15}$$

Thus, for d_{32} follows the expression

$$\frac{d_{32}}{D_1} = \frac{P(d)}{\varphi}We^{-3/5} = C_6We^{-3/5} \tag{16}$$

Murakami and Minemura [11] proposed a different but more sophisticated correlation for the Weber number. In this correlation the Weber number is related to the impeller and is defined by the angular velocity ω, the radius of the leading edge R_1 and the blade spacing H_1.

$$We_\mathrm{I} = \frac{\rho_\mathrm{c}\omega^2R_1^2H_1}{\sigma} \tag{17}$$

The influence of the number of blades is considered in H_1. The blade spacing is given by

$$H_1 = \frac{\pi D_1}{Z_\mathrm{b}} \tag{18}$$

where Z_b is the number of blades. If the number of blades increases while the impeller dimensions remain the same, the Weber number decreases. The basic experiments are described in [11].

At low rotational speeds and high flow rates, for instance in the operating mode of serial connected centrifugal pumps, particle break-up mainly takes place in areas of accelerated flow in the discharge nozzle. Therefore, an alternative definition of the Weber number is introduced to describe the two-phase flow in the centrifugal pump discharge nozzle at low pump frequencies. Studies from Håkansson and Innings [25] confirm that there is a dependency of energy dissipation zone from rotational speed represented by:

$$We_\mathrm{D} = \frac{\rho_\mathrm{c}v_\mathrm{d}^2D_\mathrm{h}}{\sigma} \tag{19}$$

The mean flow speed at the volute throat is described by v_d and D_h corresponds to the hydraulic diameter at the volute throat.

Additionally, the SMD can be correlated with the maximum stable droplet diameter d_max. In their study on evaluation of models for droplet shear effect of centrifugal pumps, Dabirian et al. [15] have shown that the SMD can be calculated from the maximum stable droplet diameter d_max with

$$d_{32} = 0.4d_\mathrm{max} \tag{20}$$

2.4 Droplet Size Distributions

For the analysis of L/L multiphase flows, DSDs are determined experimentally and approximated by DSD functions. The cumulative number frequency $Q_\mathrm{n}(d_\mathrm{k})$ and the cumulative volume frequency $Q_\mathrm{v}(d_\mathrm{k})$ are obtained by plotting the total amount and volume of particles in dependence of their particle class size d_k (Eq. (21)) [26].

$$Q_\mathrm{n}(d_\mathrm{k}) = \frac{\sum_{i=1}^{k} n_\mathrm{i}d_\mathrm{i}}{\sum_{j=1}^{M} n_\mathrm{j}d_\mathrm{j}}$$

and (21)

$$Q_\mathrm{v}(d_\mathrm{k}) = \frac{\sum_{i=1}^{k} n_\mathrm{i}d_\mathrm{i}^3}{\sum_{j=1}^{M} n_\mathrm{j}d_\mathrm{j}^3}$$

Here, n_i is the number of droplets, which are summarized in a size class i with diameter d_i, d_k is the diameter of the droplets in the k^{th} size class, which is between class 1 and M. For the special case that $k = M$, $Q_n(d_M) = 1$ and $Q_v(d_M) = 1$. The control variable j is introduced to differ from i for summing up all size classes of j. The number density frequency $q_n(d_i)$ and the volume density frequency $q_v(d_i)$ can be determined using Eq. (22) [26].

$$q_n(d_i) = \frac{n_i}{\sum_{j=1}^{M} n_j}$$

and (22)

$$q_v(d_i) = \frac{n_i d_i^3}{\sum_{j=1}^{M} n_j d_j^3}$$

If experimental data is log-normally distributed, the cumulative distribution function of the volumetric distribution is given by Eq. (23) and the probability density function by Eq. (24):

$$Q_v(d_i) = \frac{1}{2}\left[1 + \mathrm{erf}\left(\frac{\ln(d_i) - \mu_v}{\sqrt{2}\sigma_v}\right)\right] \tag{23}$$

$$q_v(d_i) = \frac{1}{d_i \sigma_v \sqrt{2\pi}} \exp\left(-\frac{(\ln(d_i) - \mu_v)^2}{2\sigma_v^2}\right) \tag{24}$$

where μ_v is the mean and σ_v is the standard deviation of the logarithmic values corresponding to the particle volume. Furthermore, the mean expected average volumetric value m_v and the corresponding variance v_v of the distribution are defined by μ_v and σ_v:

$$m_v = \exp\left(\mu_v + \frac{\sigma_v^2}{2}\right) \tag{25}$$

$$v_v = \exp\left(2\mu_v + \sigma_v^2\right)\left(\exp\left(\sigma_v^2\right) - 1\right) \tag{26}$$

Thus, with the knowledge of the mean m_v and the variance v_v, the droplet volumes of a log-normal DSD can be determined. Analogously, the Eqs. (21)–(26) can be applied to determine the number density frequency $q_n(d_i)$ and the cumulative number frequency $Q_n(d_i)$.

Dabirian et al. [15] applied the probability density function for log-normally distributed system in combination with Pereyra's model for the maximum stable droplet diameter (Eq. (10)), the rotational speed dependent model for the averaged energy dissipation rate (Eq. (4)) as well as the functional relationship between the SMD and the maximum stable droplet diameter (Eq. (20)) obtained from their study to predict the log-normal DSD and compare the results with the experimental data.

For the experimental data set considered in their work, Dabirian et al. [15] have proposed the following functional relationship for the mean μ_v and the standard deviation σ_v:

$$\mu_v = \ln(d_{max}) - 1.645\sigma_v \tag{27}$$

$$\sigma_v = 0.485 \tag{28}$$

3 Material and Methods

In this section, the experimental setup as well as the measurement techniques and experimental data processing methods are presented. Two experimental setups were established, one at TU Kaiserslautern and one at RWTH Aachen University. At RWTH Aachen University, the integral fluid dynamics of multiphase flow are investigated. At the TU Kaiserslautern, additionally, local multiphase phenomena in centrifugal pumps are studied in order to quantify droplet break-up. The joint work enabled valid measurements with different approaches and led to the model-based description of droplet break-up phenomena in centrifugal pumps.

3.1 Experimental Setup

To investigate the droplet break-up phenomena in centrifugal pumps, a suitable experimental setup was designed and established at both research institutions. A schematic sketch of the measuring section of the test facility is depicted in Fig. 1.

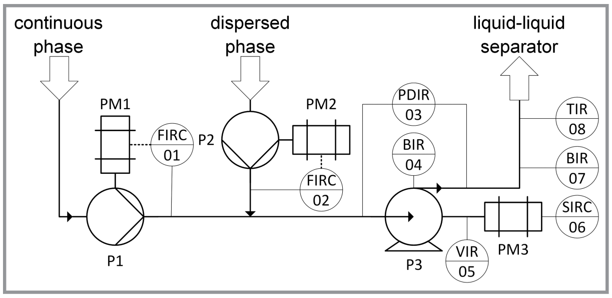

Figure 1. Measuring section of the experimental setup showing centrifugal pump and measurement instrumentation.

The primary task of this test facility is the production of a L/L dispersion at defined operating parameters such as rotational speed, total volumetric flow rate and dispersed phase fraction. A booster pump (P1) conveys the continuous phase, consisting of demineralized water, from a collecting tank to the centrifugal test pump (P3). An additional pump (P2) injects the dispersed phase, consisting of paraffin oil, into the horizontal suction pipe of the test pump (P3). The test system properties are listed in Tab. 1.

The volumetric flow rates of both phases and thus the dispersed phase fraction are adjusted by frequency converters, which are connected to the mass/volumetric flow meters (FIRC01 and FIRC02) and the pumps (P1 and P2). The rotational speed of the test pump (P3) is controlled by an additional frequency converter (SIRC06). The L/L dispersion generated by the test pump (P3) is then transported to a L/L separator and separated into the both phases, which are then stored in separate collecting tanks.

Regarding the test pump (P3), a radial centrifugal pump, type FPE 3402 (Fristam Pumpen KG, Hamburg, Germany)

Table 1. Test system properties.

Substance*	Viscosity ν [mm^{2}s^{-1}]	Density ρ [kg m^{-3}]	Interfacial tension** σ [mN m^{-1}]
FC 2006*	10.6	826	47.1
deionized water	0.893	997	

*paraffin oil (Fauth GmbH & Co. KG, Mannheim, Germany), **to deionized water. Densities measured with a density meter, type DMA 55 (Anton Paar, Austria), viscosities measured with Ubbelohde (ASTM) capillary viscosimeters (SCHOTT Instruments GmbH, Heidelberg, Germany), interfacial tensions measured via optical contact measurement, type OCA 15EC (DataPhysics Instruments GmbH, Filderstadt, Germany)

is installed in the test facility at RWTH Aachen University. A transparent replica of the FPE 3402 centrifugal pump is integrated into the test facility at TU Kaiserslautern. The housing and impeller dimensions of the FPE 3402 centrifugal pump are given in the Supporting Information (SI). Furthermore, a transparent replica of a radial centrifugal pump, type MPN 101 (Schmitt Kreiselpumpen GmbH & Co. KG, Ettlingen, Germany) is applied at TU Kaiserslautern. A detailed description of the transparent replica of MPN 101 centrifugal pump as well as the test facility located at TU Kaiserslautern are shown in Schmitt et al. [14]. The similar design of the test facilities allows the comparison of the droplet breakup phenomena between the FPE 3402 centrifugal pump and its transparent replica. Furthermore, the different measurement techniques and data processing methods applied at both research institutions can be compared to each other.

3.2 Measurement Techniques and Data Processing Methods

3.2.1 TU Kaiserslautern

A differential pressure sensor (PDIR03), type Digibar (Endress+Hauser Group Services AG, Reinach, Switzerland) is installed for determination of the pump head. A torque sensor (VIR05), type DRDL-II-5-0.5-w (ETH-Messtechnik GmbH, Gschwend, Germany) is installed between the electric motor and the pump shaft in order to determine the torque at the pump shaft during the mixing process. The electromagnetic flowmeter OPTIFLUX 5300 (KROHNE Messtechnik GmbH, Duisburg, Germany) was used for speed regulation of the booster pump. Data from differential pressure sensor, torque sensor, rotational speed measurements and flowmeter are recorded via acquisition system in LabView® (National Instruments, Austin, TX, USA). Details about the uncertainty of the measurement devices are given in Tab. S1 in the SI. The optical multimode online probe (OMOP) (TU Kaiserslautern, Germany) was used for the investigation of the transparent replica of the FPE 3402 centrifugal pump (P3) in respect of multiphase applications. The probe (BIR07) is installed downstream of the test pump (P3) at a distance of ten times the discharge nozzle diameter of the pump. At low flows rates, depending on the rotational speed, flow recirculation may occur downstream the discharge nozzle. An OMOP measurement too close to the discharge nozzle leads to repetitive detection of circulating droplets and thus to higher deviations from the actual DSD. The OMOP is used for image acquisition of particle collectives [27]. The measuring system uses telecentric illumination with a custom-built high-performance LED and a telecentric lens for detection of droplet swarms. An AcA 1300-60gm camera (Basler AG, Ahrensburg, Germany) with a set resolution of 1280 × 1024 pixels and a maximum frame rate of 60 fps was used. A high-speed camera, type Os8 (Integrated design tools Inc, USA) was used to investigate breakup phenomena within the transparent test pump (BIR04) at different positions. Motion Studio (Integrated Design Tools Inc, USA) was used to record the fluid flow in the pump housing. Sufficient lighting was provided by a high-power LED panel (TU Kaiserslautern, Germany). Image processing was done with a convolutional neural network (CNN), optimized for particle size distribution measurements. The CNN was programmed and trained with computer generated images and applied to the experimentally generated images using the Python® (v 3.6) distribution Anaconda® in the corresponding OpenCV version. Image acquisition and processing cause deviations between actually measured and automatically evaluated DSD. An analysis of the OMOP probe images and the successive image processing, based on monodispersed droplets and DSD with known mean diameters, has led to a mean detection error of 6.4 % for SMD. A detailed description of this analysis and of this data processing method is given in Schäfer et al. [28]. An exemplary analysis of the probe images can be seen in Fig. 2a.

3.2.2 RWTH Aachen University

By means of a temperature sensor (TIR08), PT100 element and a differential pressure sensor (PDIR03), type DPT-10 (WIKA Alexander Wiegand SE & Co. KG, Klingenberg am Main, Germany) the operating parameters temperature and pressure difference are indicated and recorded via LabView® during the experiment. Operating parameters rotational speed, volumetric flow rates and dispersed phase fraction are controlled via LabView® as well. For volumetric flow rate control, the mass flow rates are measured with the Coriolis mass flow meters (FIRC01 and FIRC02), type Optimas 1400 C (KROHNE Messtechnik GmbH, Duisburg, Germany) and converted into volumetric flow rates by

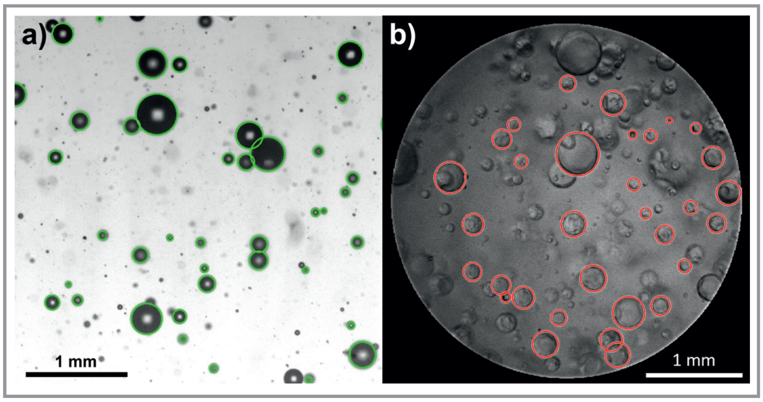

Figure 2. Example of measurement techniques and experimental data processing methods: a) OMOP + CNN, b) endoscope measuring probe + software designed in MATLAB.

means of continuous and dispersed phase densities. Details about the uncertainty of the measurement devices are given in Tab. S1. An endoscope measuring probe, type ENDO R100 038 000 50 (Olympus Deutschland GmbH, Hamburg, Germany) was used for image acquisition of L/L dispersions at the discharge nozzle of the test pump (P3). The probe (BIR07) is installed downstream of the test pump (P3) at a distance of ten times the discharge diameter of the pump, analogous to the research institution TU Kaiserslautern. The measuring system uses illumination with a high-performance LED, type F5100 Endo (Olympus Deutschland GmbH, Hamburg, Germany) and a high-speed camera, type JAI GO-5100M-USB (Stemmer Imaging AG, Puchheim, Germany) with a resolution of 2464×2056 pixels, a pixel size of 3.45 µm and a maximum frame rate of 74 fps. Common Vision Blox (Stemmer Imaging AG, Puchheim, Germany) was used for image recording. Image processing was conducted using a software designed in MATLAB® (The MathWorks, Inc., Natick, MA, USA). An exemplary analysis of the probe images can be seen in Fig. 2b. Image acquisition and processing cause deviations between actually measured and automatically evaluated DSD. To determine the deviation between manual and automatic evaluation, 100 images were evaluated manually and compared to the results of the automatic evaluation. The comparison resulted in an average detection error of 12 % regarding the Sauter mean diameter.

In order to investigate droplet break-up phenomena within the centrifugal pump as well as the DSDs at the discharge nozzle of the pumps systematically, the pump type, impeller diameter, rotational speed, volumetric flow rate of the continuous phase and dispersed phase fraction were varied. The experimental design implemented in this work can be found in Tab. 2. A detailed description of the experiments performed in the transparent replica of MPN 101 centrifugal pump is shown in Schmitt et al. [14].

4 Results and Discussion

In this section, the experimental and modeling results for SMD and droplet size distributions are presented. Two modelling approaches for SMD are discussed and compared in terms of accuracy. Furthermore, the relationship between the SMD and the parameters of a droplet size distributions are verified by means of literature data.

4.1 Sauter Mean Diameter

Fig. 3 shows the experimentally determined SMDs for the FPE 3402 centrifugal pump depending on the rotational speed and dispersed phase fraction for a continuous phase volumetric flow rate of 1.5 $m^3\,h^{-1}$ and impeller diameter of 75 mm. The results correspond to the test series A (D_2 = 75 mm), B, C and D (Tab. 2).

The experimental investigations at a dispersed phase fraction between 1 and 5 vol % were performed at TU Kaiserslautern. The experimental studies on break-up phenomena for dispersed phase fractions >5 vol % were performed at RWTH Aachen University. To ensure the comparability of the results regarding the transparent replica of the FPE 3402 centrifugal pump as well as the different measurement techniques and data processing methods, an experiment with identical parameters was performed at both research institutions. The experiment was conducted at a continuous phase volumetric flow rate of 1.5 m^3h^{-1}, an impeller diameter of 75 mm, a dispersed phase fraction of 5 vol % and a

Table 2. Experiments for different operating points.

Test series	Pump type	Impeller diameter D_2 [mm]	Rotational speed n [min^{-1}]	Vol. flow rate cont. phase $\dot{Q}$ [m^3h^{-1}]	Dispersed phase fraction θ [vol %]
A	FPE 3402	75 / 90 / 110	0–2030	1.5	1
B	FPE 3402	75	1160–2900	1.5	5
C	FPE 3402	75	1450	1.5	1–5
D	FPE 3402	75	1450	1.5	5–30
E	MPN 101	75	0–2030	0.5–0.9	1

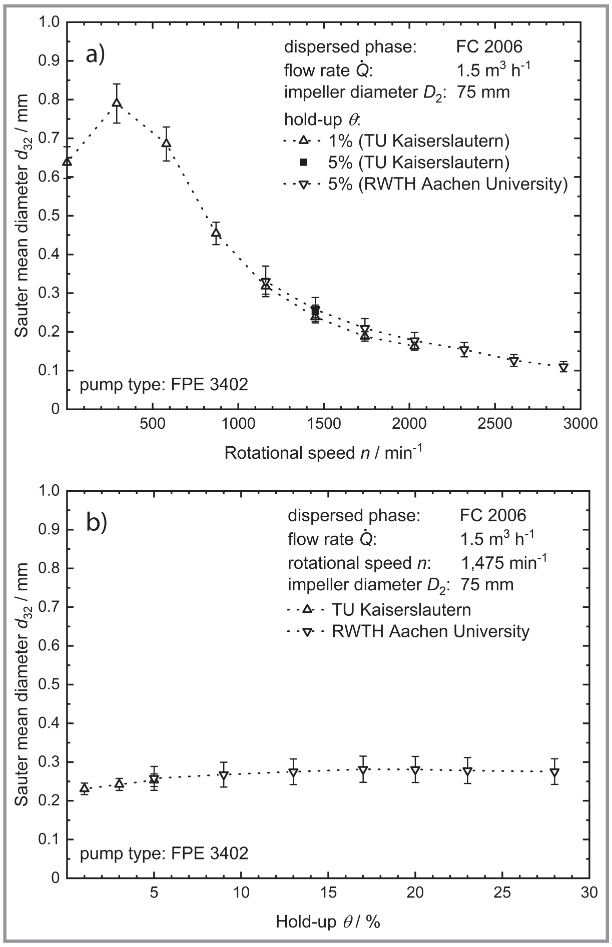

Figure 3. Experimentally determined Sauter mean diameters at the FPE 3402 centrifugal pump outlet for increasing rotational speed (a) and dispersed phase fraction (b).

rotational speed of 1450 min^{-1} (Fig. 3a). With a deviation in the measured SMD of max. 5 µm, the comparison validates that the test facilities as well as the different measurement techniques and data processing methods at both research institutions deliver comparable results. Therefore, further investigations can be divided among the both research institutions and, thus, the research institutions complement each other with the produced results.

Regarding the rotational speed (Fig. 3a), it is recognizable that the SMD at the pump outlet rises with increasing rotational speed starting from 0 min^{-1} to a maximum value at 290 min^{-1}. An explanation for the increase in Sauter mean diameter from 0 to 290 min^{-1} is the flow regime at the discharge nozzle of the centrifugal pump. Experimental investigations have shown that, depending on the flow regime and the resulting trajectory of the streamlines, drop breakage occurs mainly at the discharge nozzle (see Fig. 5). Due to the slowly rotating impeller, the droplets are hardly broken by the impeller, but the streamlines at the discharge nozzle are aligned in such a way that the droplet breakage in the discharge nozzle is disadvantaged. With an increase of rotational speed starting from 290 min^{-1}, the SMD decreases gradually. It can also be observed that a change in rotational speed has a higher influence on the SMD than a change in dispersed phase fraction (Fig. 3b). Moreover, the SMD remains almost unchanged when the dispersed phase fraction is increased from 9 to 28 vol %.

The experimental data points of test series A and E (Tab. 2) were used to determine the fitting parameters of model-based approaches for SMD (Figs. 4 and 7). Two different modeling approaches were applied in this work and compared to each other concerning the accuracy.

In the first modeling approach, Dabrian's functional relationship between the SMD and the maximum stable droplet diameter (Eq. (20)) is applied in combination with Pereyra's model for maximum stable droplet diameter (Eq. (10)) and the rotational speed dependent correlation for averaged energy dissipation rate caused by rotation of the impeller $\bar{\varepsilon}$ (Equation (4)) (Fig. 4).

Fig. 4a shows the experimental determined SMDs for the FPE 3402 centrifugal pump depending of the rotational

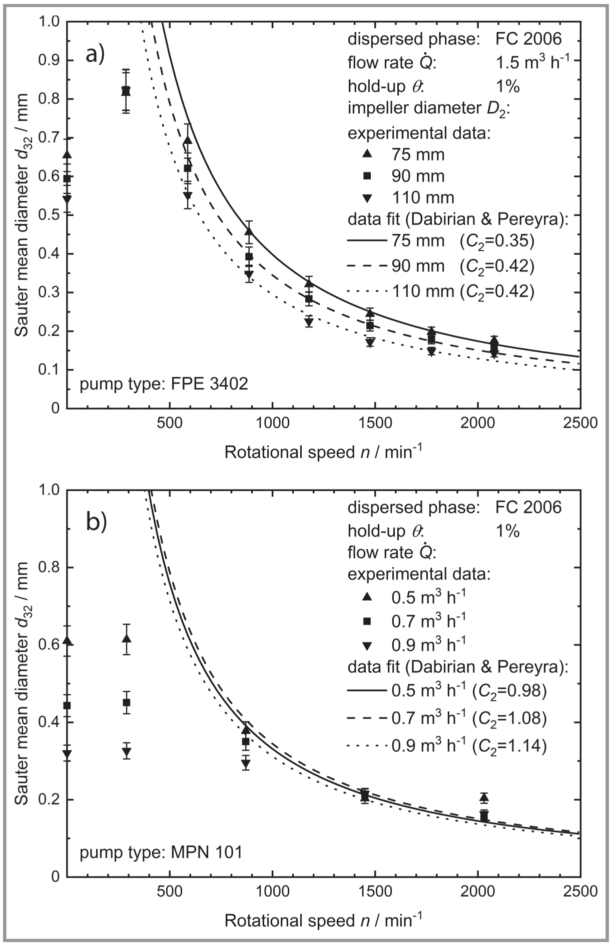

Figure 4. Sauter mean diameter in dependence on rotational speed for the FPE 3402 (a) and the MPN 101 (b) centrifugal pumps. Comparison between experimental data and model approach of Dabirian and Pereyra.

speed n at different impeller diameters D_2. The same SMD trend can be seen for all three impeller diameters. Moreover, the SMDs tend to decrease with increasing impeller diameter at constant rotational speeds. The influence of the impeller diameter D_2 decreases with increasing speed, the SMDs of all three impellers converge. The experiments shown in Fig. 4b correspond to the measured SMDs for the MPN 101 centrifugal pump in dependence of the rotational speed n at different volumetric flow rates $\dot{Q}$. The SMD coincide at high rotational speeds for all volumetric flow rates, which means that the main influencing parameter regarding the droplet size in this regime is the rotational speed. However, at low rotational speeds, the volumetric flow rate has a significant influence. Furthermore, the SMDs tend to decrease with increasing volumetric flow rate at constant rotational speeds. The increase in Sauter mean diameter at the volumetric flow rate of $0.5\,\mathrm{m^3h^{-1}}$ and rotational speed of $2030\,\mathrm{min^{-1}}$ is caused by a measurement error.

The curves in Fig. 4 present the model-based description of the SMD by means of the first modeling approach. For this purpose, the parameter C_2 of Eq. (4) was fitted to the experimentally determined maximum stable droplet diameter at rotational speeds between 886 and $2079\,\mathrm{min^{-1}}$ for the FPE 3402 pump and between 870 and $2030\,\mathrm{min^{-1}}$ for the MPN 101 centrifugal pump. The results in Fig. 4 show that the fitting parameter C_2 is mainly dependent on the impeller diameter and less on the flow rate. Furthermore, it can be noted that the experimental SMD is represented with good accuracy by the first modeling approach for rotational speeds between $580\,\mathrm{min^{-1}}$ and $2030\,\mathrm{min^{-1}}$ but is overestimated in operating range between $0\,\mathrm{min^{-1}}$ and $580\,\mathrm{min^{-1}}$. The reason for the deviations between the measured and calculated SMDs at rotational speeds lower than $580\,\mathrm{min^{-1}}$ is the underestimation of the averaged energy dissipation rates at lower rotational speeds by the model. Experimental data of the SMDs at the pump outlet for the FPE 3402 centrifugal pump show that despite low rotational speeds droplet break-up takes place within the centrifugal pump, which depends on the flow rate and the pump geometry. The transparent design of the centrifugal pump allows high-speed analyses that reveal the zones responsible for droplet break-up. Fig. 5 shows that at stationary impeller droplet break-up is initiated by the flow passing the volute throat. Large eddy structures in the discharge nozzle with droplet break-up are visible.

Therefore, at low rotational speeds, droplet break-up caused by the flow rate at the discharge nozzle becomes comparatively more frequent than droplet break-up at the impeller leading edge. However, droplet break-up caused by the volumetric flow rate is not considered in this modeling approach.

For the averaged energy dissipation rates caused by rotation of the impeller, the comparison between calculated values using Eq. (4) and experimentally determined values by means of Eq. (2) is presented in Fig. 6.

Fig. 6 shows that the determination of the averaged energy dissipation using Eq. (4) coincides very well with the averaged energy dissipation rates determined from experimental data by means of Eq. (2). The modeling of the averaged energy dissipation rates according to Eq. (2) produces slightly larger values than those determined according to Eq. (4), but both are in the same range. A deviation of the

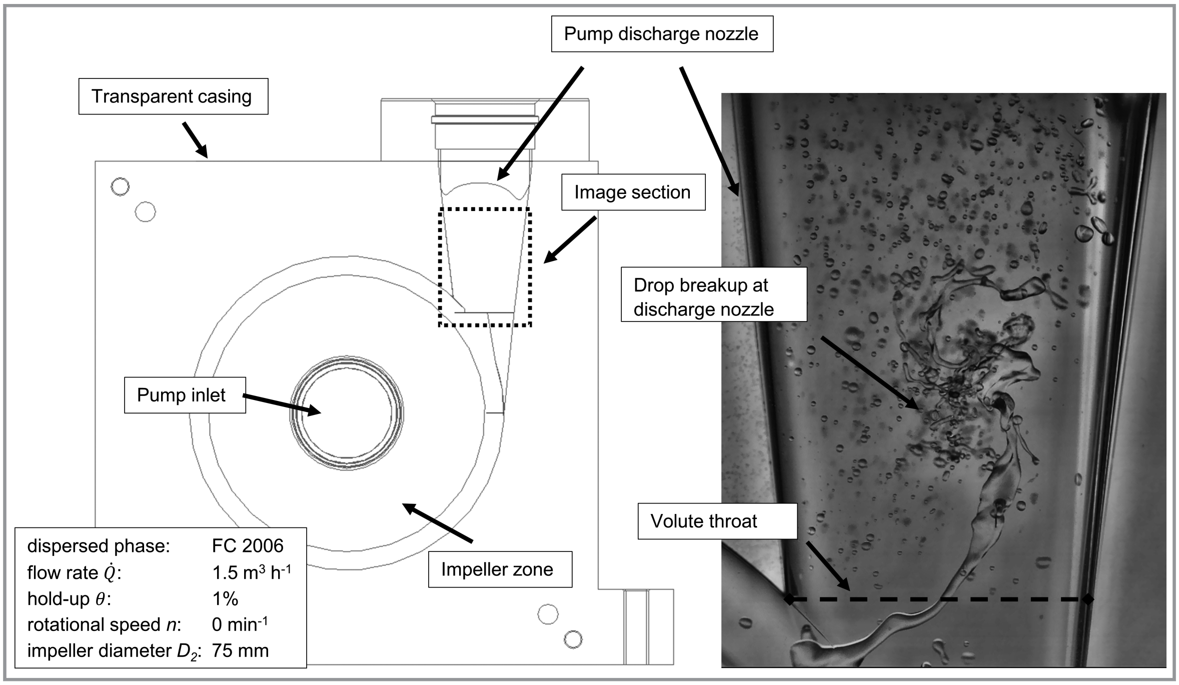

Figure 5. Droplet break-up in pump discharge nozzle at low impeller speeds for the FPE 3402 centrifugal pump.

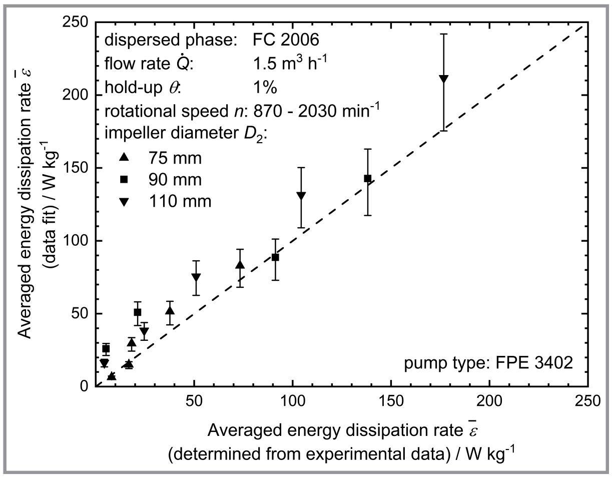

Figure 6. Comparison of averaged energy dissipation rate calculated using Eq. (4) to values determined from experimental data by means of Eq. (2).

modelled energy dissipation rate is given in Fig. 6 to quantify the influence of the measuring uncertainty of the image processing. For the determination of the averaged energy dissipation rate, the entire volume between the differential pressure measurement points (PDIR03) was used (see Fig. 1).

In the alternative modeling approach for the SMD, the functional relationship between the SMD and the Weber number (Eq. (16)) is applied in combination with Murakami's and Minemura's (Eq. (17)) as well as Håkansson's and Innings' (Eq. (19)) definitions for the Weber number (see Fig. 7). To consider the energy dissipation caused by the volumetric flow rate at low rotational speeds, Eq. (16) was adapted assuming that the maximum Weber number is decisive for the SMD:

$$\frac{d_{32}}{D_1} = C_6 \max(We_{\mathrm{I}}, We_{\mathrm{D}})^{-3/5} \tag{29}$$

The symbols in Fig. 7 show the experimentally determined SMD for the FPE 3402 and the MPN 101 centrifugal pumps in dependence of the rotational speed at different impeller diameters (Fig. 7a) and volumetric flow rates (Fig. 7b) as already introduced in Fig. 4. The curves in Fig. 7 present the model-based description of the SMD by means of the alternative modeling approach. For this purpose, the parameter C_6 of Eq. (29) was fitted to the experimentally determined SMD at a rotational speed between 886 and 2079 min^{-1}. The results in Fig. 4 show that the fitting parameter C_6 is mainly dependent on the pump geometry, e.g., impeller diameter, but independent from the volumetric flow rate. Furthermore, compared to the experimentally determined SMDs, it can be noted that the alternative modeling approach describes the SMD adequately in the entire examined operating range between 0 min^{-1} and 2030 min^{-1}.

In comparison with the first modeling approach, the reason for the better agreement between the measured and

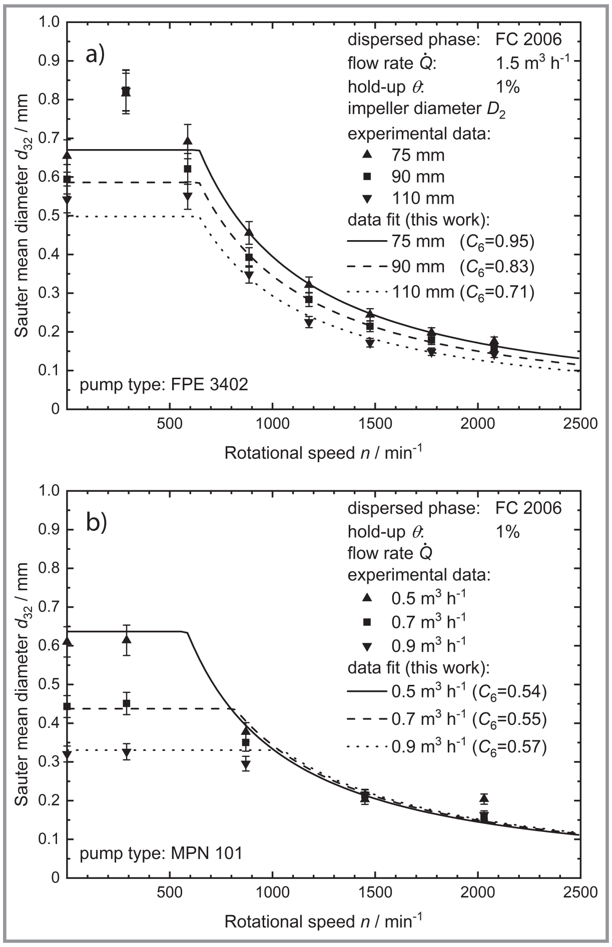

Figure 7. Sauter mean diameter in dependence on rotational speed for the FPE 3402 (a) and the MPN 101 (b) centrifugal pump. Comparison between experimental data and model approach of this work.

calculated SMDs at rotational speeds lower than 580 min^{-1} lies in the consideration of energy dissipation caused by the volume flow rate. In this rotational speed range, a volumetric flow dependent SMD is calculated by using the Weber number correlation from Eq. (19). This equation results from droplet break-up in the discharge nozzle due to the accelerated flow at the narrow flow cross-section at the volute throat and the cohesive surface tension force.

Therefore, in rotational speed range above 580 min^{-1}, the SMD is calculated by using the Weber number correlation from Eq. (17). The transition between low and high rotational speeds is realized by the Weber number approach from Eq. (29).

In conclusion, the alternative modeling approach can be applied to characterize the droplet break-up phenomena in centrifugal pumps in regard to the SMD. For this purpose, the SMD for a specific material system has to be measured in the centrifugal pump with defined design parameters at least at three operating points with different rotational speeds and a constant volumetric flow rate. The obtained results can then be used to determine the fitting parameter C_6 of the alternative modeling approach in order to describe the entire operating range.

4.2 Droplet Size Distribution

For the analysis of the DSD, for each measuring point of the FPE 3402 centrifugal pump, a sufficient amount of OMOP images were evaluated by tracking the SMD until convergence was reached. The number of detected droplets per image can vary significantly, depending on the operating conditions. Based on experience, at least 500 images are necessary to correctly reproduce all DSDs for all operating ranges of the used centrifugal pump. An exact procedure for the adequate determination of the DSD is described in Schmitt et al. [14]. Fig. 8 shows representative volume droplet distribution functions determined with about 25 000 detected droplets via the optical OMOP probe. Particularly for large droplets, a strong fluctuation between the individual size classes i can be observed. In the further course, the measured data is presented as a log-normal distribution using Eqs. (23) and (24). The MATLAB® curve fitting tool was used to determine the mean μ_v and the standard deviation σ_v from the experimental data.

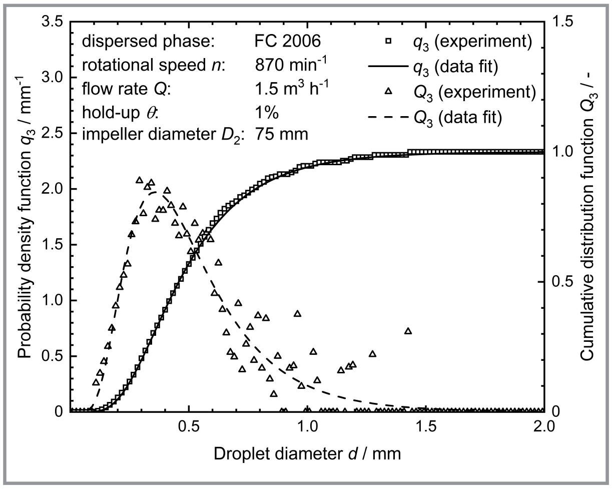

Figure 8. Characteristic DSD for the examined operating range. Comparison of experimental data and data fit for the probability density and cumulative distribution functions.

The determined mean μ_v and the standard deviation σ_v were used to calculate the mean expected average volumetric value m_v and the corresponding variance v_v by means of Eqs. (25) and (26). To identify a functional relationship between the m_v, v_v and the SMD, both parameters were plotted as a function of the SMD in double logarithmic notation (Fig. 9).

The filled symbols in Fig. 9 show the calculated values for the mean expected average volumetric value m_v (Fig. 9a) and the corresponding variance v_v (Fig. 9b) in dependence on the SMD for the examined operating range of this work.

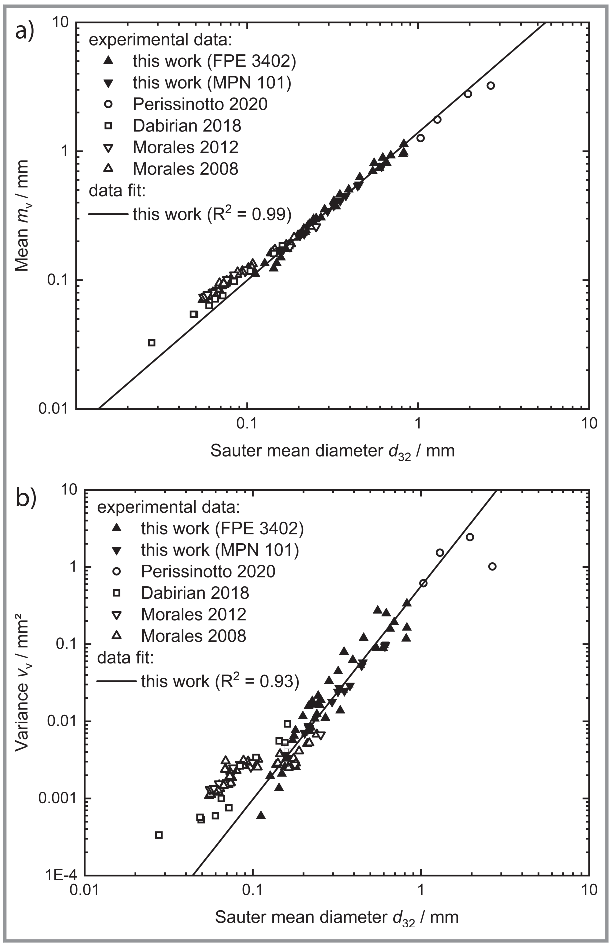

Figure 9. Mean and variance of log-normal distribution as functions of d_{32}.

It is evident that the mean expected average volumetric value as well as the corresponding variance increase with increasing SMD. Moreover, the behavior indicates a power law relationship. Therefore, experimental data of this work is used to determine the fitting parameters of an empirical relationship between m_v, v_v and the SMD. The resulting correlations are given by Eqs. (30) and (31):

$$m_v = 1.399(d_{32})^{1.147} \tag{30}$$

$$v_v = 0.566(d_{32})^{2.763} \tag{31}$$

Regarding the accuracy of the correlations, Eqs. (30) and (31) have a coefficient of determination R^2 of 0.99 and 0.93.

In conclusion, with the known SMD Eqs. (30) and (31) can be applied to determine the DSD for a defined operating point of a centrifugal pump. Furthermore, the blank symbols in Fig. 9 represent experimental data obtained from literature. For this purpose, experimental drop size distributions were extracted from the research works of Morales et al. [29], Dabirian et al. [15] and Perissinotto et al. [30] and used to determine the corresponding SMDs, the mean values and the standard deviations by means of the MATLAB® curve fitting tool. The data from literature applied to validate Eqs. (30) and (31) show a high accuracy of the correlations and their transferability to other material systems, centrifugal pump geometries and operating conditions.

5 Conclusions

In this work, investigations on droplet break-up phenomena in centrifugal pumps in dependence on material system, design and operating parameters are presented. Two experimental setups were established, one at TU Kaiserslautern and one at RWTH Aachen University. Integral fluid dynamics was investigated as well as local multiphase phenomena in centrifugal pumps were studied in order to quantify droplet break-up. Two types of centrifugal pumps and their transparent replica were used in this work. The droplet break-up phenomena within the centrifugal pump was characterized by means of the resulting SMD and DSD at the discharge nozzle of the pump. For the investigation the impeller diameter, rotational speed, volumetric flow rate of the continuous phase and dispersed phase fraction were varied systematically.

The experimental investigations on local multiphase phenomena in centrifugal pumps show that droplet break-up occurs primarily at the leading edge of the impeller. Breakage at the pump discharge nozzle is only significant at low rotational speeds and is in this case determined by the flow rate. The experimental investigations on the integral fluid dynamics show that the SMD decreases with increasing volumetric flow rate, rotational speed and impeller diameter. SMD at the pump discharge nozzle increases slightly with increasing dispersed phase fraction. Regarding the DSD, the experimental investigations show a log-normal distribution in the examined range.

Two modeling approaches for SMD are evaluated and compared in terms of accuracy. The Weber number correlation was found to be the most accurate as it describes drop break-up in a physically correct way over the whole rotational speed range. The parameters of a log-normal distribution function were adjusted to the experimentally determined DSD. A relationship between the SMD and the parameters of a log-normal distribution function was identified. Moreover, the resulting correlations were successfully validated with literature data. Thereby, the transferability of the correlations to other material systems, centrifugal pump geometries and operating conditions was shown. Furthermore, the correlations were shown to predict the DSD with high accuracy. With the established modeling approach droplet break-up phenomena in centrifugal pumps in regard to the SMD can be characterized. With the known SMD, a prediction of DSD for a defined operating point of a centrifugal pump is possible.

In future work, further material systems and design parameters, e.g., number of blades will be investigated to enhance the scope of correlations shown in this work and to show the transferability of the correlations to other pump designs. Furthermore, mass transfer will be subject of future investigations to show whether a centrifugal pump can be considered and operated specifically as an L/L extractor.

Supporting Information

Supporting Information for this article can be found under DOI: https://doi.org/10.1002/cite.202000180.

The authors would like to thank the German Federation of Industrial Research Federation (AiF) and the German Federal Ministry for Economic Affairs and Energy (BMWi) for funding our research in the involved project “Dispergier- und Koaleszierphänomene in Zentrifugalpumpen” (DisKoPump). Open access funding enabled and organized by Projekt DEAL.

Symbols used

C_{1-6}	[–]	dimensionless empirical constants
d	[mm]	droplet diameter
D_1	[mm]	diameter at blade leading edge
D_2	[mm]	diameter at blade trailing edge
d_{32}	[mm]	Sauter mean diameter
$d_{50,\mathrm{v}}$	[mm]	median value of volumetric cumulative droplet size distribution
d_h	[mm]	hydraulic diameter
d_max	[mm]	maximum stable droplet diameter
$E(k)$	[m^{2}s^{-2}]	energy spectrum function
E_S	[J]	surface energy of drop
E_V	[J]	viscous energy of drop
H	[m]	pump head
h_1	[mm]	blade spacing at impeller leading edge
$H_\mathrm{B.E.P.}$	[m]	head at best efficiency point
k	[m^{-1}]	wave number
m	[mm]	mean of lognormal distribution function
M	[–]	number of classes
M'_Shaft	[Nm]	torque on pump shaft
n	[min^{-1}]	rotational speed
$P(D)$	[–]	probability of droplet with size d in equilibrium
P_Diss	[W]	dissipation power
$P_{\dot{Q}}$	[W]	pumping power
P_Shaft	[W]	power acting on pump shaft
$\dot{Q}$	[L h^{-1}]	volumetric flow rate
$\dot{Q}_\mathrm{B.E.P.}$	[m^{3}h^{-1}]	flow rate at best efficiency point

Q_n	[–]	cumulative number frequency
q_n	[mm^{-1}]	number density frequency
Q_v	[–]	cumulative volume frequency
q_v	[mm^{-1}]	volume density frequency
r_1	[mm]	radius of impeller leading edge
r_2	[mm]	radius of impeller trailing edge
u_c	[m s^{-1}]	average fluctuation velocity
V	[m^3]	pump volume
v	[mm^2]	variance of lognormal distribution function
v_D	[m s^{-1}]	velocity at discharge nozzle (volute throat)
We_{crit}	[–]	critical Weber number
We_D	[–]	discharge nozzle Weber number
We_I	[–]	impeller Weber number
Y	[m^{2}s^{-2}]	specific energy
Z_b	[–]	number of blades

Greek symbols

μ_v	[mm]	mean of volumetric logarithmic values
ε	[m^{2}s^{-3}]	energy dissipation rate
$\bar{\varepsilon}$	[m^{2}s^{-3}]	averaged energy dissipation rate
ν_d	[mm^{2}s^{-1}]	kinematic viscosity of dispersed phase
ρ_c	[kg m^{-3}]	density of continuous phase
ρ_d	[kg m^{-3}]	density of the dispersed phase
σ	[mN m^{-1}]	interfacial tension of dispersed phase to continuous phase
σ_v	[–]	standard deviation of volumetric logarithmic values
φ	[–]	unknown functional relationship
ω	[rad s^{-1}]	angular velocity
$\tau_{intertial}$	[N m^{-2}]	inertial stress
$\tau_{interfacial}$	[N m^{-2}]	interfacial stress
β_1	[°]	blade inlet angle
β_2	[°]	blade outlet angle
θ	[vol %]	holdup

Abbreviations

CFD	computational fluid dynamics
CNN	convolutional neural network
DSD	droplet size distribution
L/L	liquid/liquid
OMOP	optical multimode online probe
SMD	Sauter mean diameter
Vol.	volumetric

References

[1] R. E. Sanders, *Chemical process safety: Learning from case histories*, 3rd ed., Elsevier Butterworth Heinemann, Amsterdam **2005**.

[2] A. Eggert, S. Sibirtsev, D. Menne, A. Jupke, *Chem. Eng. Res. Des.* **2017**, *127*, 170–179. DOI: https://doi.org/10.1016/j.cherd.2017.09.005

[3] A. Eggert, T. Kögl, W. Arlt, A. Jupke, *Chem. Eng. Res. Des.* **2019**, *142*, 143–153. DOI: https://doi.org/10.1016/j.cherd.2018.11.034

[4] M. Weber, *Chem. Ing. Tech.* **2019**, *91 (11)*, 1515–1521. DOI: https://doi.org/10.1002/cite.201800174

[5] A. J. Stepanoff, *Centrifugal and axial flow pumps: Theory, design, and application*, 2nd ed., Krieger, Malabar, FL **1993**.

[6] A. T. Troskolański, S. Łazarkiewicz, *Kreiselpumpen: Berechnung und Konstruktion*, 1st ed., Lehr- und Handbücher der Ingenieurwissenschaften, Vol. 34, Springer Basel AG, Basel **2014**.

[7] J. R. Blake, D. C. Gibson, *Annu. Rev. Fluid Mech.* **1987**, *19 (1)*, 99–123. DOI: https://doi.org/10.1146/annurev.fl.19.010187.000531

[8] X.-w. Luo, B. Ji, Y. Tsujimoto, *J. Hydrodyn.* **2016**, *28 (3)*, 335–358. DOI: https://doi.org/10.1016/S1001-6058(16)60638-8

[9] H. Keck, M. Sick, *Acta Mech.* **2008**, *201 (1–4)*, 211–229. DOI: https://doi.org/10.1007/s00707-008-0060-4

[10] S. R. Shah, S. V. Jain, R. N. Patel, V. J. Lakhera, *Procedia Eng.* **2013**, *51*, 715–720. DOI: https://doi.org/10.1016/j.proeng.2013.01.102

[11] M. Murakami, K. Minemura, *J. Fluids Eng.* **1983**, *105 (4)*, 382–388. DOI: https://doi.org/10.1115/1.3241015

[12] J. L. Turpin, J. F. Lea, J. L. Bearden, *Gas-liquid flow through centrifugal pumps: Correlation of data*, Turbomachinery Laboratories, Department of Mechanical Engineering, Texas A&M University **1986**. DOI: https://doi.org/10.21423/R1M11K

[13] R. M. Perissinotto, W. Monte Verde, M. S. d. Castro, J. L. Biazussi, V. Estevam, A. C. Bannwart, *Exp. Therm. Fluid Sci.* **2019**, *105*, 11–26. DOI: https://doi.org/10.1016/j.expthermflusci.2019.03.009

[14] P. Schmitt, M. W. Hlawitschka, H.-J. Bart, *Chem. Ing. Tech.* **2020**, *262 (4)*, 12215. DOI: https://doi.org/10.1002/cite.201900105

[15] R. Dabirian, S. Cui, I. Gavrielatos, R. Mohan, O. Shoham, in *ASME 2018 5th Joint US-European Fluids Engineering Division Summer Meeting*, Vol. 1, ASME, New York **2018**. DOI: https://doi.org/10.1115/FEDSM2018-83318

[16] H. T. Chen, S. Middleman, *AIChE J.* **1967**, *13 (5)*, 989–995. DOI: https://doi.org/10.1002/aic.690130529

[17] R. V. Calabrese, T. P. K. Chang, P. T. Dang, *AIChE J.* **1986**, *32 (4)*, 657–666. DOI: https://doi.org/10.1002/aic.690320416

[18] F. B. Sprow, *Chem. Eng. Sci.* **1967**, *22 (3)*, 435–442. DOI: https://doi.org/10.1016/0009-2509(67)80130-1

[19] J. O. Hinze, *AIChE J.* **1955**, *1 (3)*, 289–295. DOI: https://doi.org/10.1002/aic.690010303

[20] E. J. Pereyra, *Modeling of integrated compact multiphase separation system (CMSS$^{©}$)*, Dissertation, The University of Tulsa **2011**.

[21] M. Stieß, *Mechanische Verfahrenstechnik – Partikeltechnologie 1*, Springer, Berlin **2009**.

[22] J. T. Davies, *Chem. Eng. Sci.* **1985**, *40 (5)*, 839–842. DOI: https://doi.org/10.1016/0009-2509(85)85036-3

[23] R. A. Mugele, H. D. Evans, *Ind. Eng. Chem.* **1951**, *43 (6)*, 1317–1324. DOI: https://doi.org/10.1021/ie50498a023

[24] P. A. Davidson, *Turbulence: An introduction for scientists and engineers*, Oxford University Press, Oxford **2010**.

[25] A. Håkansson, F. Innings, *Chem. Eng. Process.* **2017**, *115*, 46–55. DOI: https://doi.org/10.1016/j.cep.2017.01.007

[26] E. L. Paul, V. A. Atiemo-Obeng, S. M. Kresta, *Handbook of industrial mixing: Science and practice*, Wiley-Interscience, Hoboken, NJ **2004**.

[27] M. Mickler, H.-J. Bart, *Chem. Ing. Tech.* **2013**, *85 (6)*, 901–906. DOI: https://doi.org/10.1002/cite.201200139

[28] J. Schäfer, P. Schmitt, M. W. Hlawitschka, H.-J. Bart, *Chem. Ing. Tech.* **2019**, *91 (11)*, 1688–1695. DOI: https://doi.org/10.1002/cite.201900099

[29] R. Morales, E. Pereyra, S. Wang, O. Shoham, *SPE J.* **2013**, *18 (01)*, 172–178. DOI: https://doi.org/10.2118/163055-PA

[30] R. M. Perissinotto, W. Monte Verde, C. E. Perles, J. L. Biazussi, M. S. d. Castro, A. C. Bannwart, *Exp. Therm. Fluid Sci.* **2020**, *112*, 109969. DOI: https://doi.org/10.1016/j.expthermflusci.2019.109969

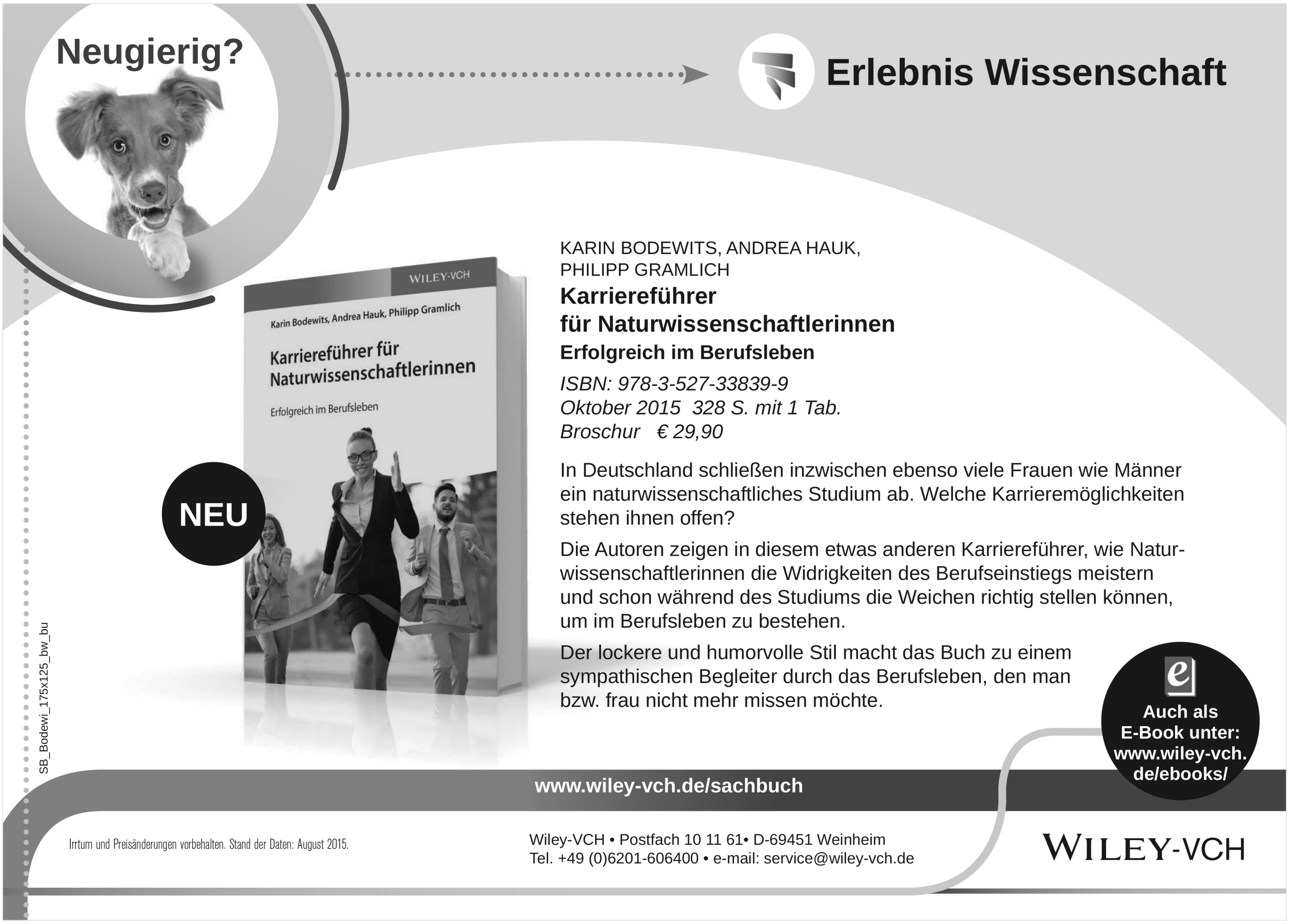

Neugierig?
Erlebnis Wissenschaft
NEU
WILEY-VCH
Karin Bodewits, Andrea Hauk, Philipp Gramlich
Karriereführer für Naturwissenschaftlerinnen
Erfolgreich im Berufsleben
SB_Bodewi_175x125_bw_bu

KARIN BODEWITS, ANDREA HAUK,
PHILIPP GRAMLICH

Karriereführer
für Naturwissenschaftlerinnen
Erfolgreich im Berufsleben

ISBN: 978-3-527-33839-9
Oktober 2015 328 S. mit 1 Tab.
Broschur € 29,90

In Deutschland schließen inzwischen ebenso viele Frauen wie Männer ein naturwissenschaftliches Studium ab. Welche Karrieremöglichkeiten stehen ihnen offen?

Die Autoren zeigen in diesem etwas anderen Karriereführer, wie Naturwissenschaftlerinnen die Widrigkeiten des Berufseinstiegs meistern und schon während des Studiums die Weichen richtig stellen können, um im Berufsleben zu bestehen.

Der lockere und humorvolle Stil macht das Buch zu einem sympathischen Begleiter durch das Berufsleben, den man bzw. frau nicht mehr missen möchte.

Auch als E-Book unter: www.wiley-vch.de/ebooks/

www.wiley-vch.de/sachbuch

Irrtum und Preisänderungen vorbehalten. Stand der Daten: August 2015.

Wiley-VCH • Postfach 10 11 61• D-69451 Weinheim
Tel. +49 (0)6201-606400 • e-mail: service@wiley-vch.de

WILEY-VCH